Electronically tunable silicon photonic delay lines

Saeed Khan,[1] Mohammad Amin Baghban,[2] and Sasan Fathpour[1,2,*]

[1]*Department of Electrical Engineering and Computer Science, University of Central Florida, Orlando, FL 32816 USA*

[2]*CREOL, The College of Optics and Photonics, University of Central Florida, Orlando, FL 32816 USA*

[*]*fathpour@creol.ucf.edu*

Abstract: Electronically tunable optical true-time delay lines are proposed. The devices utilize the combination of apodised gratings and the free-carrier plasma effect to tune the enhanced delay of silicon waveguides at a fixed wavelength. Three variations of the proposed scheme are studied and compared. The compact and integrable devices can achieve tuning ranges as high as ~660 ps with a loss of < 2.2 dB when operated in the reflection mode of the gratings. A delay of ~40 ps with a loss of < 10 dB and an estimated operation bit rate of ~20 Gb/s can be achieved.

OCIS codes: (250.0250) Optoelectronics; (250.5300) Photonic integrated circuit.

References and links

1. J. L. Corral, J. Marti, J. M. Fuster, and R. I. Laming, "True time-delay scheme for feeding optically controlled phased-array antennas using chirped-fiber gratings," IEEE Photon. Technol. Lett. **9**(11), 1529–1531 (1997).
2. Y. Okawachi, M. A. Foster, X. Chen, A. C. Turner-Foster, R. Salem, M. Lipson, C. Xu, and A. L. Gaeta, "Large tunable delays using parametric mixing and phase conjugation in Si nanowaveguides," Opt. Express **16**(14), 10349–10357 (2008).
3. E. Choi, J. Na, S. Ryu, G. Mudhana, and B. Lee, "All-fiber variable optical delay line for applications in optical coherence tomography: feasibility study for a novel delay line," Opt. Express **13**(4), 1334–1345 (2005).
4. V. Italia, M. Pisco, S. Campopiano, A. Cusano, and A. Cutolo, "Chirped fiber Bragg gratings for electrically tunable delay lines," IEEE J. Sel. Top. Quantum Electron. **11**(2), 408–416 (2005).
5. M. Pisco, S. Campopiano, A. Cutolo, and A. Cusano, "Continuously variable optical delay line based on a chirped fiber Bragg grating," IEEE Photon. Technol. Lett. **18**(24), 2551–2553 (2006).
6. B. Ortega, J. L. Cruz, J. Capmany, M. V. Andrés, and D. Pastor, "Analysis of a microwave time delay based on a perturbed uniform fiber Bragg grating operating at constant wavelength," J. Lightwave Technol. **18**(3), 430–436 (2000).
7. S. Yegnanarayanan, P. D. Trinh, F. Coppinger, and B. Jalali, "Compact silicon-based integrated optic time delays," IEEE Photon. Technol. Lett. **9**(5), 634–635 (1997).
8. J. Yang, N. K. Fontaine, Z. Pan, A. O. Karalar, S. S. Djordjevic, C. Yang, W. Chen, S. Chu, B. E. Little, and S. J. B. Yoo, "Continuously tunable, wavelength-selective buffering in optical packet switching networks," IEEE Photon. Technol. Lett. **20**(12), 1030–1032 (2008).
9. A. Melloni, F. Morichetti, C. Ferrari, and M. Martinelli, "Continuously tunable 1 byte delay in coupled-resonator optical waveguides," Opt. Lett. **33**(20), 2389–2391 (2008).
10. J. Cardenas, M. A. Foster, N. Sherwood-Droz, C. B. Poitras, H. L. R. Lira, B. Zhang, A. L. Gaeta, J. B. Khurgin, P. Morton, and M. Lipson, "Wide-bandwidth continuously tunable optical delay line using silicon microring resonators," Opt. Express **18**(25), 26525–26534 (2010).
11. A. Melloni, A. Canciamilla, C. Ferrari, F. Morichetti, L. O'Faolain, T. F. Krauss, R. De La Rue, A. Samarelli, and M. Sorel, "Tunable delay lines in silicon photonics: coupled resonators and photonic crystals, a comparison," IEEE Photon. J. **2**(2), 181–194 (2010).
12. F. Xia, L. Sekaric, and Y. Yurii, "Ultracompact optical buffers on a silicon chip," Nat. Photonics **1**(1), 65–71 (2007).
13. F. Morichetti, A. Melloni, C. Ferrari, and M. Martinelli, "Error-free continuously-tunable delay at 10 Gbit/s in a reconfigurable on-chip delay-line," Opt. Express **16**(12), 8395–8405 (2008).
14. Y. Q. Jiang, W. Jiang, X. Chen, L. Gu, B. Howley, and R. T. Chen, "Nano-photonic crystal waveguides for ultra-compact tunable true time delay lines," Proc. SPIE **5733**, 166–175 (2005).
15. J. Adachi, N. Ishikura, H. Sasaki, and T. Baba, "Wide range tuning of slow light pulse in SOI photonic crystal coupled waveguide via folded chirping," IEEE J. Sel. Top. Quantum Electron. **16**(1), 192–199 (2010).
16. M. S. Rasras, C. K. Madsen, M. A. Cappuzzo, E. Chen, L. T. Gomez, E. J. Laskowski, A. Griffin, A. Wong-Foy, A. Gasparyan, A. Kasper, J. Le Grange, and S. S. Patel, "Integrated resonance-enhanced variable optical delay lines," IEEE Photon. Technol. Lett. **17**(4), 834–836 (2005).

#143117 - $15.00 USD Received 28 Feb 2011; revised 18 May 2011; accepted 25 May 2011; published 2 Jun 2011

17. G. Bjork and O. Nilsson, "A new exact and efficient numerical matrix theory of complicated laser structures: properties of asymmetric phase-shifted DFB lasers," J. Lightwave Technol. **5**(1), 140–146 (1987).
18. J. Hong, W. Huang, and T. Makino, "On the transfer matrix method for distributed-feedback waveguide devices," J. Lightwave Technol. **10**(12), 1860–1868 (1992).
19. T. Makino, "Effective-index matrix analysis of distributed feedback semiconductor lasers," J. Lightwave Technol. **28**, 434–440 (1992).
20. P. Yeh, *Optical Waves in Layered Media* (Wiley, New York, 1988), p. 102.
21. R. A. Soref and B. R. Bennett, "Kramers-Kronig analysis of E-O switching in silicon," Proc. SPIE **704**, 32–37 (1986).
22. S. Fathpour, K. K. Tsia, and B. Jalali, "Two-photon photovoltaic effect in silicon," J. Lightwave Technol. **3**, 1211–1217 (2007).
23. T. Erdogan, "Fiber grating spectra," J. Lightwave Technol. **15**(8), 1277–1294 (1997).
24. N. A. Riza, M. A. Arain, and S. A. Khan, "Hybrid analog–digital variable fiber-optic delay line," J. Lightwave Technol. **22**(2), 619–624 (2004).
25. G. P. Agrawal, *Fiber-optic communication systems* (Wiley, New York, 2002), p. 26.
26. A. Ghatak and K. Thyagarajan, *Introduction to fiber optics* (Cambridge, UK, 1898), p. 257.
27. G. Jiang, R. Chen, Q. Zhou, J. Yang, M. Wang, and X. Jiang, "Slab-modulated sidewall Bragg gratings in silicon-on-insulator ridge waveguides," IEEE Photon. Technol. Lett. **23**, 6–8 (2011).
28. X. Wang, W. Shi, R. Vafaei, N. A. F. Jaeger, and L. Chrostowski, "Uniform and sampled Bragg gratings in SOI strip waveguides with sidewall corrugations," IEEE Photon. Technol. Lett. **23**, 290–292 (2011).
29. S. Ahn and J. Lee, J. Kim, S. Kim, S. H. Lee, J. Park and P. Yoon, "Fabrication of subwavelength aluminum wire grating using nanoimprint lithography and reactive ion etching," Microelectron. Eng. **78–79**, 314–318 (2005).
30. B. D. Lucas, J.-S. Kim, C. Chin, and L. J. Guo, "Nanoimprint lithography based approach for the fabrication of large-area, uniformly oriented plasmonic arrays," Adv. Mater. (Deerfield Beach Fla.) **20**(6), 1129–1134 (2008).
31. S. Grego, A. Huffman, M. Lueck, B. R. Stoner, and J. Lannon, "Nanoimprint lithography fabrication of waveguide-integrated optical gratings with inexpensive stamps," Microelectron. Eng. **87**(10), 1846–1851 (2010).
32. M. L. Povinelli, S. G. Johnson, and J. D. Joannopoulos, "Slow-light, band-edge waveguides for tunable time delays," Opt. Express **13**(18), 7145–7159 (2005).
33. J. H. Schmid, P. Cheben, S. Janz, J. Lapointe, E. Post, A. Delage, A. Densmore, B. Lamontagne, P. Waldron, and D.-X. Xu, "Subwavelength grating structures in silicon-on-insulator waveguides," in Advances in Optical Technologies **2008**, Article ID 685489, Hindawi Publishing Corporation, 2008.

1. Introduction

Tunable optical true-time delay lines are essential components in optical beam-forming control of phased-array antennas (PAAs) [1], in optical communication networks [2] and in optical coherence tomography [3]. Mostly, chirped fiber grating is being used as a dispersive element for these applications. In these devices, the desired tunability is achieved by varying the wavelength of the driving laser [1]. However, the need for synchronous tunable laser sources and tunable bandpass filters makes these systems complicated [4]. Delay of fiber Bragg gratings at a constant wavelength can be tuned by temperature control, applying mechanical strain or magnetic field [4–6]. All these fiber-based schemes, however, suffer from bulkiness, slow response and/or low time resolution. Hence, integrated photonics on glass and semiconductors has been considered for tunable delay lines. Particularly, silicon (Si) photonics is an attractive platform, as reviewed in the following.

Optical delays as high as 100 ps with an accuracy of ~0.5 ps have long been demonstrated in silicon waveguides [7]. All-pass filters (APFs) and coupled resonator optical waveguides (CROW) are two common resonant-type structures that have been pursued more recently on silicon and other materials [8–13]. Also, photonic crystal (PhC) line-defect waveguides have been proposed and implemented for optical delays [11,14,15]. To tune the delay in these structures, thermo-optic effect is typically used [11,15,16]. However, thermo-optics is a slow effect and it is challenging to control the temperature rise only to the locality of such tiny structures. In one report based on APFs, for instance, the response time was ~1 ms [8]. Unresolved issues also exist regarding the efficiency of the mechanism used to deliver heat. More importantly, APFs, CROWs and PhC waveguides suffer from high optical losses. In a report by IBM, for example, for a delay of 200-500 ps, the loss of APFs and CROWs was 22-23 dB, while 4-cm-long bent (spiral) submicron waveguides had a much less loss of 7 dB (1.7 dB/cm) [12]. PhC devices also suffer from high insertion losses (as high as 64 dB/cm [14] or 35-100 dB/ns [11,15]). The optical loss, attainable optical delay and operating data rate of these pursued technologies are summarized in Table 1.

#143117 - $15.00 USD Received 28 Feb 2011; revised 18 May 2011; accepted 25 May 2011; published 2 Jun 2011

Table 1: Comparison of the State of the Art Silicon Delay Line Techniques.

Device type	Optical loss (dB/ns)	Delay (ps)	Data rate (Gb/s)
APF	43 [12]	510 [12]	5 [12]
CROW	35-105 [11,12]	220 [12]	4-25 [11,12]
PhC waveguides	35-100 [11,15]	72 [15]	25 [11]

Evidently, simultaneous achievement of a low-loss, fast, compact, wavelength-independent, high-resolution and electronically-tunable optical delay line is lacking. Such a novel class of devices is proposed here. The device can offer a reasonable tradeoff between size (length) and optical loss. That is, the employed waveguide-grating-based devices may not be as compact as CROW-, APF-, or PhC-based approaches, but they are expected to attain significantly lower insertion losses. A major advantage is that, for the first time, tuning is induced electronically rather than thermally. The tunability is achieved at a constant wavelength via the free-carrier plasma effect.

2. Methodology

The schematic of the proposed devices are shown in Fig. 1. They consist of a silicon-on-insulator (SOI) rib waveguide straddled with a *p-n* junction diode and three different types of gratings. In all cases, while keeping the incident wavelength fixed, applying a forward voltage to the *p-n* junction varies the refractive index of the rib waveguide through free-carrier plasma effect. Consequently, the change in the refractive index blue shifts the whole delay spectrum of the device. As a result, the delay in the reflected light will increase or decrease depending on the slope of the delay spectrum at the operating wavelength. As will be explained later, apodized gratings need to be used rather than uniform gratings. Two types of Gaussian profiles (labeled as "mesa" and "grooved" in Figs. 1(a) and (b)) and a raised-cosine profile (Fig. 1(c)) were used for the widths of the gratings.

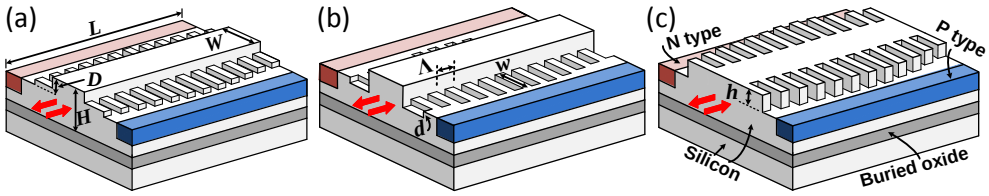

Fig. 1. Structures of (a) mesa-type (b) grooved-type and (c) chirped raised-cosine-type tunable optical delay lines on SOI. The varying widths of the gratings emphasize the corresponding apodised profiles used. None of the schematics are in scale. In all devices L = 2 cm, W = 1.5 μm, H = 2 μm, D = 0.9 μm and Λ = 224 nm. Regarding other shown dimensions: (a) h = 50 nm, w = 85 nm; (b) d = 50 nm, w = 55 nm; (c) h = D = 0.9 μm and w = 460 nm.

The delay of the reflected light, τ, was calculated from the phase derivative approach, i.e.,

$$\tau = \frac{d\theta}{d\omega} = -\frac{\lambda^2}{2\pi c}\frac{d\theta}{d\lambda},$$

where θ is the phase of the reflection coefficient and λ is the incident wavelength. The reflection coefficients of the structures were calculated using the transfer matrix method [17–20]. The method was chosen due to its reasonably small computation time. Its accuracy was confirmed by comparing it with the coupled-mode theory for one of the structures.

The effective refractive index of each corrugated section was determined using the commercial RSoft simulator. A commercial electronic device simulator, ATLAS by Silvaco, was used to determine the carrier concentration in the rib waveguide corresponding to the applied forward bias across its *p-n* junction. Soref's expression [21,22] was used to determine the carrier-induced refractive index change in silicon structure at around the Bragg wavelength of 1550 nm. Non-chirped Gaussian and chirped raised-cosine grating structures were simulated. The rib waveguide dimensions and material parameters were borrowed from

#143117 - $15.00 USD Received 28 Feb 2011; revised 18 May 2011; accepted 25 May 2011; published 2 Jun 2011

Ref [22]. Briefly, the waveguide width $W = 1.5$ μm, the rib height (SOI thickness), $H = 2$ μm and the etch depth (ridge height) is $D = 0.9$ μm. In all of the devices, the waveguide length, $L = 2$ cm and the corrugation period of the side grating is $\Lambda = 224$ nm.

To get large delays, it is necessary to have long gratings. However, this leads to impractically sharp variation of the delay spectrum around the operating wavelength. Therefore, to get a smooth delay spectrum, one needs to apodise the grating width [23]. A Gaussian profile with a full-width at half maximum (FWHM) of 2.66 cm was used for the mesa-type structure (Fig. 1 (a)) with a maximum grating width, w, of 85 nm and a height, h, of 50 nm. For the grooved-type device $w = 55$ nm and the grating depth $d = 50$ nm. The same FWHM of 2.66 cm was used for the grooved-type device. A third class of devices, i.e., with a mesa-type grating structures but with a third-order raised-cosine function width of $\cos^3(\pi z/L)$ (for $-L/2 < z < L/2$), is also studied for comparison. $w = 460$ nm and h is equal to the mentioned waveguide etched depth of 0.9 μm (see Fig. 1(c)). These values are much higher than the grooved and mesa cases in order to achieve a higher change in refractive index contrast that is needed for high delays. A chirp rate of -22.4×10^{-2} nm/cm was used to comply with the requirements of high delay and appropriate slope of delay versus wavelength.

3. Results and discussions

The optical loss induced by the injected free carriers can become a disadvantage compared to chirped fiber gratings, which typically have a loss of less than 0.5 dB [24]. One reason various types of devices are studied here is to find an optimum structure that yields the highest possible time delay with the lowest possible loss. Inevitably, a limit in the maximum carrier injection level had to be set to limit the free-carrier loss within an acceptable range. Accordingly, a maximum refractive index variation, and hence variation in optical delay, can be achieved when the diode bias is varied. The devices presented here operate in the reflection mode of the grating. It is noteworthy that the device can be used in the transmission mode, as well. Transmission mode may be useful for some system applications where delay lines need to be cascaded or adding optical circulators is not desirable [24]. However, higher optical delays are achievable in the reflection mode, which is what reported here.

Figures 2(a) and (b) show the delay and the reflectivity spectra for the Gaussian device types at 0 V and at the bias that gives maximum delay, V_{max}, when the insertion loss is limited to 3 dB. Evidently, at either bias the reflectivity remains high, as desired for reflection mode operation. By an increase in the applied voltage, the refractive index decreases due to the free-carrier plasma effect, which in turn blue-shifts the whole delay spectrum. The blue-shift in the spectrum of the device will increase or decrease the delay in the reflected light depending on whether the rising edge (positive slope) or falling edge (negative slope) of the delay spectrum occurs in the vicinity of the operating wavelength. If the slope is positive and the incident wavelength is fixed at the lowest wavelength value in the tuning range, the delay in the reflected light will increase with an increase in the applied voltage (see Fig. 2(d)). The opposite is true for the negative slope case. The mesa-type Gaussian device possesses a positive slope (Fig. 2 (a)) at the operating wavelength, while the grooved-type Gaussian (Fig. 2 (b)) and mesa-typed chirped raised-cosine devices (Fig. 2(c)) have negative slopes. In the case of Fig. 2(c), the very high coupling coefficient of the grating results in a very broadband and high reflectivity in the shown detuning range of –1 to –1.15 nm at both 0 and V_{max}, thus the reflectivity superimpose and appear flat (~100%).

#143117 - $15.00 USD Received 28 Feb 2011; revised 18 May 2011; accepted 25 May 2011; published 2 Jun 2011

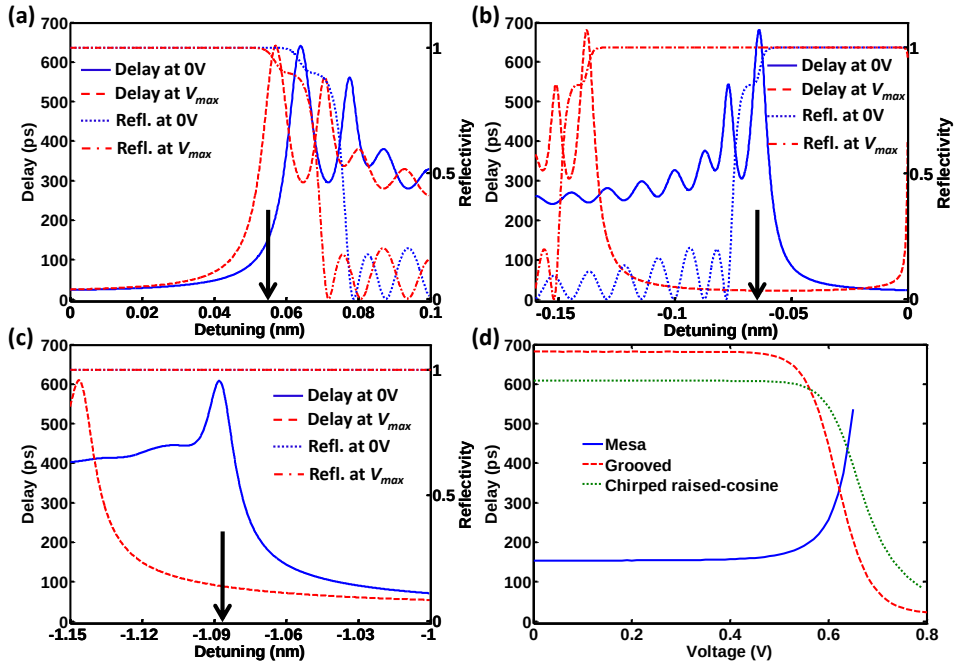

Fig. 2. Delay and reflectivity spectrum of (a) mesa-type Gaussian device, (b) grooved-type Gaussian device, (c) chirped raised-cosine device, at 0 V and at V_{max} when the insertion loss is limited to 3 dB. The arrows show the operating wavelengths. The reference of the detuning axis (0 nm) is the Bragg wavelength set at 1550 nm. Reflectivities at 0 V and at V_{max} are identical in case (c) thus appear superimposed; (d) Delay versus voltage characteristics for the three types of devices when the insertion loss is limited to 3 dB.

The two negative-slope devices offer higher range of tunable optical delay as compared with the positive-slope (mesa-type Gaussian) device. To explain this, it is reminded that in all devices, increasing the bias voltage blue shifts the delay spectra. To comply with the aforementioned free-carrier loss limit, the operating wavelength ought to be set such that the maximum delay occurs at V_{max} for the positive-slope device, whereas it occurs at 0 V for the negative-slope devices (see Fig. 2). As the applied voltage increases from 0 V in the positive-slope device, the incident light effectively travels deeper into the waveguide before being reflected. The combination of this increasing travel path and increasing free-carrier loss limits the tuning range of the device to ~480 ps. In contrast, the carrier injection is very small at 0 V in the negative-slope devices, i.e., the longest time delay at this bias is attributed to long travel path but with low free-carrier loss. At high biases, although there is large free-carrier absorption per unit volume, the light travel path is small and hence the overall undesired impact of free-carrier loss is less than the positive-slope case. As a result, the grooved-type Gaussian grating device of Fig. 1(b) offers the highest tunability range of ~660 ps. Figure 2(d) shows optical delay versus voltage plots for the mesa, grooved and raised-cosine types of devices.

Figure 3(a) shows the tunable time delay versus insertion loss in the same devices. Insertion loss includes the linear loss (0.5 dB/cm [22]), the free-carrier absorption [21,22], and the reflectivity loss of the gratings (see Fig. 2) but excludes the coupling loss in and out of the waveguides. When the bias voltage increases from 0 V in the grooved-type device, the light travel path decreases and delay decreases accordingly until the loss reaches a minimum of 0.58 dB at 0.73 V. After this point, the delay does not decrease as much but the free-carrier loss increase at a faster pace, therefore loss starts increasing to a final value of 0.92 dB at V_{max} = 0.80 V. All the other presented trends in Fig. 3(a) can be similarly explained by considering how fast the delay and the loss vary, with respect to each other, as the bias changes.

#143117 - $15.00 USD Received 28 Feb 2011; revised 18 May 2011; accepted 25 May 2011; published 2 Jun 2011

The dispersion-induced limit on the bit rate for a non-return-to-zero (NRZ) modulation format was calculated based on standard models [25,26]. Only the results on the grooved-type device, which attains the highest delay range, are presented here. In order to maximize the bit rate, it was necessary to deviate from the aforementioned grating FWHM of 2.66 cm, i.e., it is varied from 0.33 to 2.66 cm. The inset of Fig. 3(b) shows the dispersion curve versus wavelength detuning from the Bragg wavelength for these lowest and highest values of FWHM. It is evident that a flatter dispersion can be achieved with the choice FWHM = 0.33 cm. There is a classic tradeoff between tunable delay and bandwidth when both are plotted versus various values of grating FWHM (Fig. 3(b)). For operating at > 20 Gb/s, a maximum delay of ~40 ps is predicted with a loss of 10 dB. In the other extreme of the plots, very high tunability (as high as 660 ps) is attainable with losses as low as 2.2 dB but of course the bit rate will become very low (1.6 Gb/s).

It is noteworthy that for FWHM between 0.83 cm and 1.66 cm (corresponding to bit rate of ~4.6 and ~9 Gb/s), extra caution has to be considered because in this range the voltage dependency of delay will be oscillatory. That is smooth and monotonically decreasing plots such as those in Fig. 2(d) for the grooved-type device cannot be conveniently achieved.

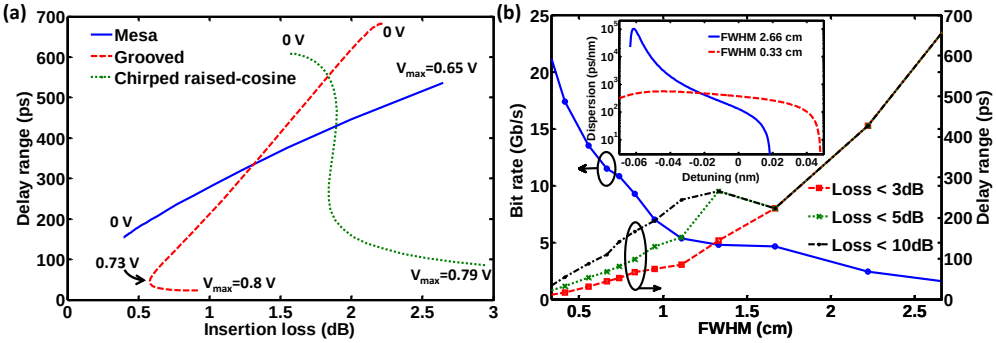

Fig. 3. (a) Delay versus insertion loss characteristics of the three types of devices; (b) Bit rate and tunable delay range versus the FWHM of the Gaussian profile grating in the case of the grooved-type device. The inset shows the dispersion versus detuing for FWHM of 2.66 cm (highest delay) and 0.33 cm (highest bit rate).

It should be finally noted that electron-beam lithography may not be conveniently applicable for fabrication and mass production of the long gratings (~ 2 cm) required here. Fortunately, both deep-ultraviolet optical lithography [27,28] and nanoimprinting lithography [29–31] are capable of patterning the feature sizes aimed in this work.

4. Conclusions

In summary, new class of electronically-tunable optical true-time delay lines is proposed that can compromise the tradeoff between the loss and the size of the devices on SOI platform. Apodised gratings are used to increase the time delay of waveguides, which physically resembles the slow-light effects in PhC waveguides [32]. Although the group index increase may not be as dramatic as in photonic crystals, the advantage is a lower propagation loss expected in waveguide gratings [33]. The grooved-type devices proposed here have the highest achievable tunable delay range (~ 660 ps) along with the lowest loss (< 2.2 dB). This corresponds to a loss per unit time delay of ~3.3 dB/ns, which is certainly advantageous over the state-of-the-art technologies summarized in Table 1. The grooved-type devices can operate at > 20 Gb/s with a tunable delay of ~40 ps, which is acceptable for optical beamforming control of a 7-bit PAA system at the X-band (8-12 GHz) with a longest delay line of 2.56 ns [1,24].

#143117 - $15.00 USD Received 28 Feb 2011; revised 18 May 2011; accepted 25 May 2011; published 2 Jun 2011